PNAS RESEARCH ARTICLE | IMMUNOLOGY AND INFLAMMATION

Tumor resistance to anti-mesothelin CAR-T cells caused by binding to shed mesothelin is overcome by targeting a juxtamembrane epitope

X.F. Liu[a], M. Onda[a], J. Schlomer[b], L. Bassel[b], S. Kozlov[b], C.-H. Tai[a], Q. Zhou[a], W. Liu[a], H.-E. Tsao[a], R. Hassan[c], M. Ho[a], and I. Pastan[a,1]

Contributed by I. Pastan; received October 6, 2023; accepted November 27, 2023; reviewed by Stephen Gottschalk and Michael G. Rosenblum

Despite many clinical trials, CAR-T cells are not yet approved for human solid tumor therapy. One popular target is mesothelin (MSLN) which is highly expressed on the surface of about 30% of cancers including mesothelioma and cancers of the ovary, pancreas, and lung. MSLN is shed by proteases that cleave near the C terminus, leaving a short peptide attached to the cell. Most anti-MSLN antibodies bind to shed MSLN, which can prevent their binding to target cells. To overcome this limitation, we developed an antibody (15B6) that binds next to the membrane at the protease-sensitive region, does not bind to shed MSLN, and makes CAR-T cells that have much higher anti-tumor activity than a CAR-T that binds to shed MSLN. We have now humanized the Fv (h15B6), so the CAR-T can be used to treat patients and show that h15B6 CAR-T produces complete regressions in a hard-to-treat pancreatic cancer patient derived xenograft model, whereas CAR-T targeting a shed epitope (SS1) have no anti-tumor activity. In these pancreatic cancers, the h15B6 CAR-T replicates and replaces the cancer cells, whereas there are no CAR-T cells in the tumors receiving SS1 CAR-T. To determine the mechanism accounting for high activity, we used an OVCAR-8 intraperitoneal model to show that poorly active SS1-CAR-T cells are bound to shed MSLN, whereas highly active h15B6 CAR-T do not contain bound MSLN enabling them to bind to and kill cancer cells.

immunotherapy | cancer | antibody | pancreatic cancer | ovarian cancer

Significance

This paper describes humanized Chimeric Antigen Receptor T (CAR-T) cells that target mesothelin (MSLN) but do not bind to shed MSLN and are ready for clinical development. They cause complete remissions in several animal models including a difficult-to-treat pancreatic cancer PDX (patient derived xenograft) model. The study reveals the mechanism accounting for very high anti-tumor activity in mice: failure to bind shed MSLN in ascites of mice with ovarian cancer.

CAR-T therapy has shown remarkable success in treating B cell malignancies and multiple myeloma (1–4). However, the development of CAR-T therapy for solid tumors has been less successful, and no CAR-T cells for solid tumors have been Food and Drug Administration (FDA) approved (4, 5). Mesothelin (MSLN) is a glycoprotein which is highly expressed on the surface of many types of cancers, including mesothelioma, and cancers of the ovary, pancreas, lung, and stomach, but not expressed on essential organs (6, 7). This pattern of expression makes MSLN a very popular target for CAR-T and other antibody-based cancer therapies (8–11). MSLN is shed from tumor cells and is found inside tumors and in ascites, where the levels are very high (12–14). Shed MSLN in the blood is a potential biomarker for cancer detection (15, 16). Shed MSLN, particularly inside tumors and in ascites, should be able to inactivate many anti-MSLN therapies before the agents reach the target cell. These include whole antibodies, antibody-drug conjugates, bispecific antibodies, and CAR-T cells. Thus, shed MSLN appears to be a major impediment to the success of antibody-based therapies. We recently described an anti-MSLN antibody, 15B6, that binds to MSLN at the cell membrane (Fig. 1*A*) and does not bind to shed MSLN (Fig. 1*B*), (17). The Fv of Mab 15B6 makes very active CAR-T cells that kill MSLN expressing tumor cells and produce complete regressions in solid tumor models (17). We compared its activity with CAR-T cells made with the SS1 Fv that binds at the amino terminus of shed MSLN and cell-bound MSLN (Fig. 1*B*). We observe that the SS1 CAR-T have very low anti-tumor activity in mice and attribute the low activity to shed MSLN binding to and inactivating SS1 CAR-T cells (17).

We have now humanized the mouse Fv and shown that CAR-T cells made with the humanized Fv (h15B6 Fv) are as effective in cell killing and inducing complete tumor regressions. Using these humanized CAR-T cells, we directly demonstrate that they replicate inside tumors and in the ascites of tumor-bearing mice. In mouse ascites, shed MSLN is attached to low-activity SS1-CAR-T cells hindering their ability to bind to and kill cancer cells, whereas shed MSLN is not attached to high-activity 15B6 CAR-T cells.

Results

Humanized CAR-T Construction. To humanize the Fv region of 15B6, we tried several approaches and found that using the closest human germline sequences as a guide was the most successful. In Fig. 1*C*, the C-terminal peptide N584 – S598 in orange is complexed

Author affiliations: [a]Laboratory of Molecular Biology, National Cancer Institute, NIH, Bethesda, MD 20892; [b]Center for Advanced Preclinical Research, Frederick National Lab for Cancer Research Center for Cancer Research, National Cancer Institute, NIH, Frederick, MD 21701; and [c]Thoracic and Gastrointestinal Malignancies Branch, National Cancer Institute, NIH, Bethesda, MD 20892

Author contributions: X.F.L., S.K., M.H., and I.P. designed research; X.F.L., J.S., Q.Z., W.L., and H.-E.T. performed research; M.O., L.B., R.H., and M.H. contributed new reagents/analytic tools; C.-H.T. and I.P. analyzed data; and X.F.L., S.K., and I.P. wrote the paper.

Reviewers: S.G., St. Jude Children's Research Hospital; and M.G.R., UT MD Anderson Cancer Center.

Competing interest statement: X.F.L., M.O., M.H., and I.P. are inventors on patents on 15B6 antibody and have assigned all rights to NIH. One of the reviewers (M.G.R.) of this paper is working with a company that has licensed an anti-MSLN antibody (designated SD1) from NIH that was discovered by NIH employee M.H., a co-author of this paper.

[1]To whom correspondence may be addressed. Email: pastani@mail.nih.gov.

This article contains supporting information online at https://www.pnas.org/lookup/suppl/doi:10.1073/pnas.2317283121/-/DCSupplemental.

Published January 16, 2024.

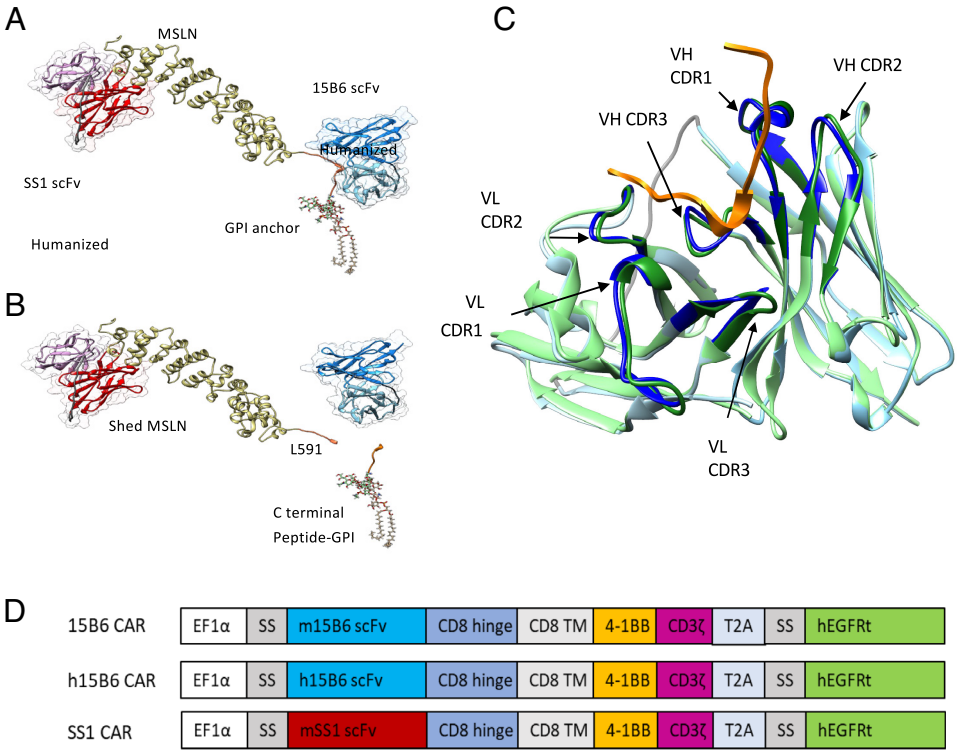

Fig. 1. Illustration of MSLN and CAR-Ts organization. (*A* and *B*) Structural model of MSLN connected to GPI anchor bound by the two humanized scFvs: 15B6 and SS1, used in CAR-T studies. The MSLN (PDB ID 7UED_M) is in olive green; the C-terminal MSLN residues N584 to S598 (PDB ID 7U8C_BA2) in orange are the epitopes where 15B6 binds. The light chain, linker, and heavy chain of the humanized 15B6 and SS1 scFv, modeled by AlphaFold2, are shown in ribbon and surface drawing in light blue, dark gray, blue, pink, dark gray, and red, respectively. The complex was made by superposing scFv15B6 and scFvSS1 models to 7U8C, 4F3F, and 7UED. (*C*) Comparison of mouse and humanized 15B6 structures. The MSLN C-terminal peptide N584 – S598 is in orange, complexed with mouse 15B6 Fv in green (PDB ID 7U8C). Humanized scFv 15B6 modeled by AlphaFold2 is in blue, superposed with mouse 15B6 Fv. CDR regions are in darker colors and labeled. The RMSD between the two 15B6s calculated by TM-align is 0.85 Å with TM-score 0.98 and all 223 Fv residues aligned, except the 15 residues linker colored in gray. (*D*) Schematic showing expression vectors used to make CAR-T cells. SS, signal sequence; hEGFRt contains domains III and IV and transmembrane domain.

with mouse 15B6 Fv in green (PDB ID 7U8C). Humanized scFv 15B6 modeled by AlphaFold2 is in blue, superposed with mouse 15B6 Fv. CDR regions are in darker colors and labeled. The RMSD between the two 15B6s calculated by TM-align is 0.85 Å with TM-score 0.98, and all 223 Fv residues are aligned, except for the 15-residue linker colored in gray. This result

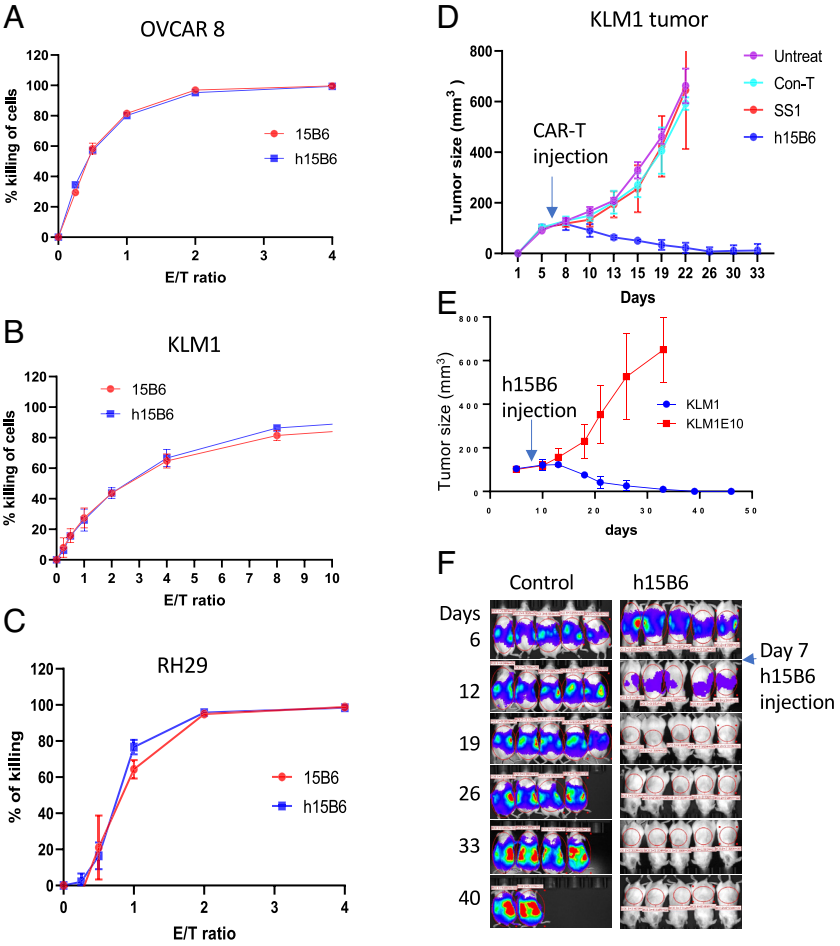

Fig. 2. Humanized 15B6 CAR-T cells have the same activity as CAR-T with mouse Fv. (*A–C*) Cell killing assays comparing h15B6 with either mouse 15B6 or SS1 CAR-T using OVCAR 8 (*A*), KLM1 (*B*) or RH29 cells (*C*). n = 3 (*A–C*). h15B6 CAR-T cause complete regressions of KLM1 tumors in NSG mice. SS1 CAR-T and control T cells have no activity, n = 5. (*D*) h15B6 CAR-T give complete responses in KLM1 subcutaneous tumors expressing MSLN but not in a MSLN knock out line (KLM1 E10), n = 5. (*E*) h15B6 CAR-T give complete responses in an intraperitoneal OVCAR 8 model. KLM1 injected 5 million, KLM1E10 injected 0.1 million. Tumor size was measured twice a week. OVCAR8-luc cells were implanted IP. Five millions of h15B6 CAR-T were injected on day 7. Tumors were imaged every week as described in the Methods section.

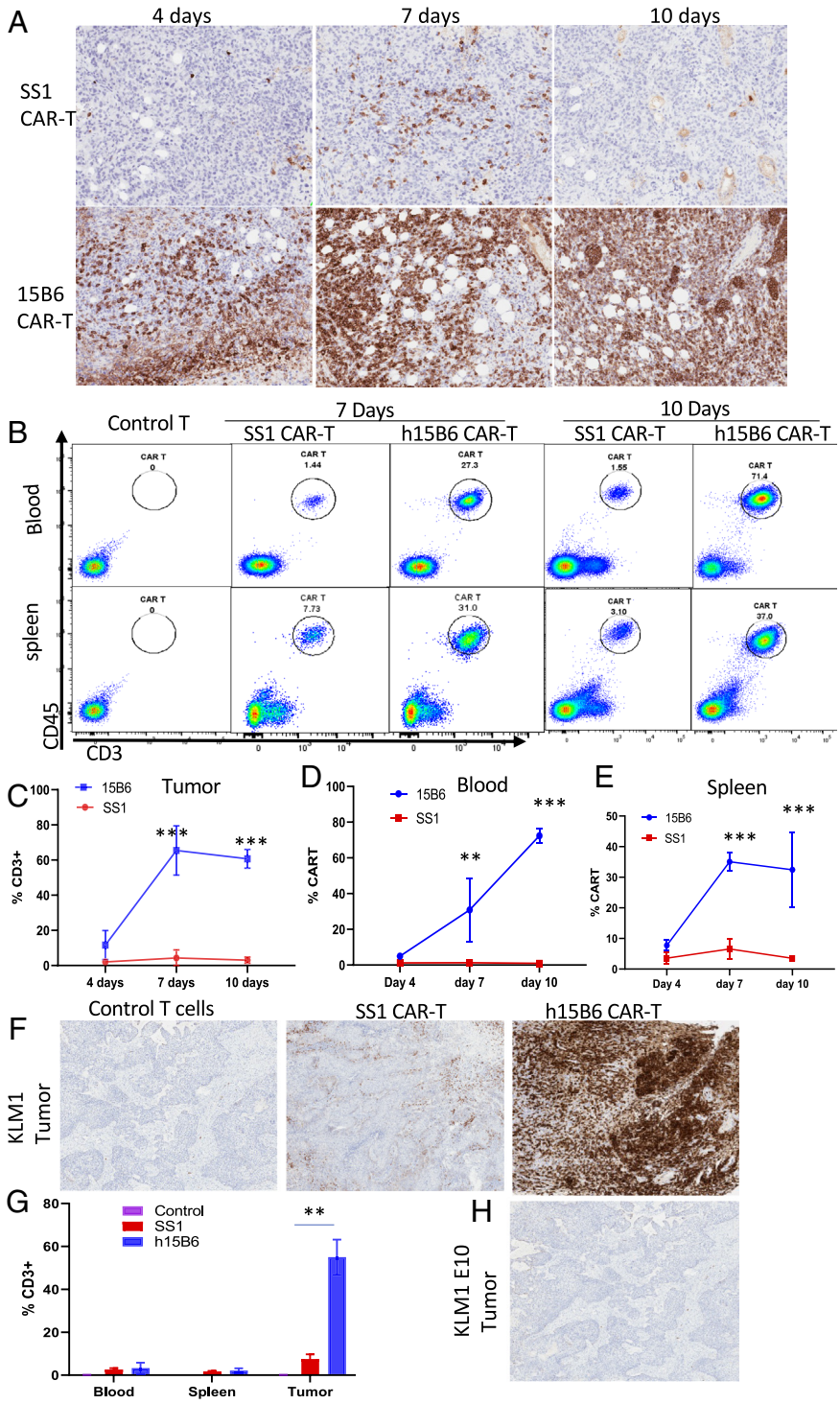

Fig. 3. h15B6 CAR-T cells, but not SS1 CAR-T cells, accumulate in tumors. (*A*) Mice received 5 million OVCAR-8 cells I.P., and on day 21, the mice were imaged and treated with 10 million of either SS1 or h15B6 CAR-T cells. After 4, 7, or 10 d of treatment, tumors were removed for IHC analysis with anti-CD3. (*B*) On days 7 and 10, spleen and blood cells were analyzed by flow cytometry using anti-CD3 and anti-CD45. All cells were first gated with DAPI for live cells; then, CD3 and CD45 double-positive cells were identified as indicated by circles. (*C*) In the *Left* panel, CD3-positive cells from A were analyzed using HALO imaging, and % of CD3-positive cells is shown in the graph. (*D* and *E*) show % CAR-T in blood and spleen (N = 3). (*F*) Mice with KLM1 subcutaneous tumors were injected with either control T cells, SS1 CAR-T, or h15B6 CAR-T 7 d (when tumor reached 100 mm^3) after tumor implantation. Seven days later, tumors were removed and analyzed by IHC staining with anti-CD3, (*G*) Percentage of CD3-positive cells in blood, spleen, or tumor (n = 3). (*H*) KLM1 E10 MSLN KO cells were implanted as in *A*, and after 7 d of 15B6 CAR-T treatment, tumors were removed and stained with anti-CD3, showing that there is no h15B6 CAR-T present in the tumor. $^{**}P < 0.01$; $^{***}P < 0.001$.

indicates that the Fv structure is very likely not changed by the humanization process and the Fv should bind to MSLN like the original Mab. Fig. 1 *A* and *B* and *SI Appendix*, Fig. S1 show the amino acid sequence of the humanized Fv and its alignment with the original mouse Fv and the human germline sequences used to guide humanization. Sequences changed from mouse to human are shown in blue boxes. To assess the affinities of mouse and humanized Mab 15B6, we employed mass photometry in which the antibody and antigen are in solution in their native form (18). We find that m15B6 (Kd 23.5 nM) has a slightly higher affinity than h15B6 (Kd 57.8 nM) as shown in *SI Appendix*, Fig. S2)

h15B6 CAR-T and m15B6 CAR-T Have Similar Anti-Tumor Activity. h15B6 Fv was inserted into a CAR-T expression vector (17) and its activity was compared with the CAR-T containing the original mouse Fv SS1 that binds to the amino terminus of MSLN and is present in shed MSLN. The regions to which the antibodies bind are shown in Fig. 1 *A* and *B*. The properties of CAR-T cells containing m15B6 Fv and the h15B6 Fv are shown in Fig. 2 *A*–*C*. Their cytotoxic activities are indistinguishable on 3 different human cancer cell lines expressing MSLN. The cell lines were chosen from cancers that frequently express MSLN: OVCAR-8 (ovarian), KLM1 (pancreatic), and RH29 (mesothelioma). We tested the activity of the humanized CAR-T cells in mice using KLM1 cells growing as

subcutaneous tumors and OVCAR-8 cells growing IP mimicking the location of ovarian cancer in humans. Fig. 2*D* shows that h15B6 CAR-T produce complete remissions in the KLM1 model, whereas SS1 CAR-T have no anti-tumor activity. Fig. 2*E* shows that h15B6 CAR-T has no activity against KLM1 tumors in which the MSLN gene is knocked out establishing its specificity for tumors expressing MSLN (19). Fig. 2*F* shows that the h15B6 CAR-T cells also produce complete remissions in OVCAR-8 tumors growing IP. Images of 5 mice receiving h15B6 CAR-T cells are shown; complete remissions were observed in all the mice. These data show that CAR-T cells containing the humanized Fv have high anti-tumor activity like the CAR-T made with the mouse Fv.

Location of CAR-T in Blood, Spleen, and Tumors. We have proposed that one major reason 15B6 CAR-T cells have very high anti-tumor activity is that they do not bind to shed MSLN present in tumors and other body fluids (17). Another important reason for high anti-tumor activity is that the epitope to which the Fv binds is very close to the cell membrane (20, 21). To directly determine whether MSLN is bound to CAR-T cells in tumor-bearing mice, we first examined the distribution of h15B6 CAR-T cells in 2 tumor models: OVCAR 8 and KLM1. Fig. 3*A* shows that there are large numbers of h15B6 CAR-T cells inside OVCAR-8 tumors on day 4, 7, and 10 after CAR-T administration, but there are very few SS1 CAR-T cells at these times. There are also a large number of h15B6 CAR-T cells in the spleen and blood on day 7 and 10, but fewer SS1 CAR-T cells (Fig. 3 *B*–*E*). In KLM1 tumors on day 7, there are very few SS1 CAR-T cells and many h15B6 CAR-T cells (Fig. 3 *F* and *G*). In the blood and spleen, there are very few CAR-T cells of either type (Fig. 3*G* and *SI Appendix*, Fig. S3). We also found that h15B6 CAR-T start to accumulate in tumors on day 4 and reach a peak on day 7 (*SI Appendix*, Fig. S4). To show the tumor uptake of CAR-T cells by the KLM1 tumors is MSLN dependent, we analyzed tumors from a MSLN knock out cell line, KLM E10 (17), and found no h15B6 CAR-T in the tumors showing the need for MSLN expression (Fig. 3*H*).

Shed MSLN Binds to SS1-CAR-T But Not 15B6 CAR-T in the Ascites of Mice with OVCAR-8 Tumors. Fig. 4 *A* and *B* show that CAR-T cells are present in the ascites of mice receiving both types of CAR-T cells, but there are many more h15B6 CAR-T cells than SS1 CAR-T cells. To identify the CAR-T cells that were bound to MSLN, we employed Mab YP218 that reacts with shed MSLN and binds at a different site than SS1 Fv (10). Ascites from the peritoneal cavity of mice with OVCAR-8 tumors was removed on day 7 after CAR-T administration and analyzed for MSLN bound to the Fv of the CAR-T. Fig. 4 *C* and *D* shows that shed MSLN is bound to 34% (590/1,755) of SS1 CAR-T cells but less than 1% (67/7,519) of h15B6 CAR-T cells. To assess the ability of CAR-T cells to bind shed MSLN present in patient ascites, we incubated the CAR-T cells with ascites fluid from 4 patients with ovarian cancer or mesothelioma and measured the amount of shed MSLN bound to the CAR-T cells. With all four patient samples, we found that 44 to 50% of SS1 CAR-T cells are bound to MSLN, whereas only 2 to 3% of h15B6 CAR-T cells are bound to MSLN (Fig. 4*E* and *SI Appendix*, Fig. S5). These experiments in mice and with human ascites samples provide strong evidence for the role of shed MSLN in causing tumor resistance to CAR-T therapy.

h15B5 CAR-T Cells Produce Complete Remissions in the Pancreatic Cancer PDX (Patient Derived Xenograft) Mouse Model. Most CAR-T animal experiments are carried out in NOD Scid Gamma (NSG) mice bearing tumors derived from human cancer cell lines (5). To determine whether h15B6 CAR-T are active in a model

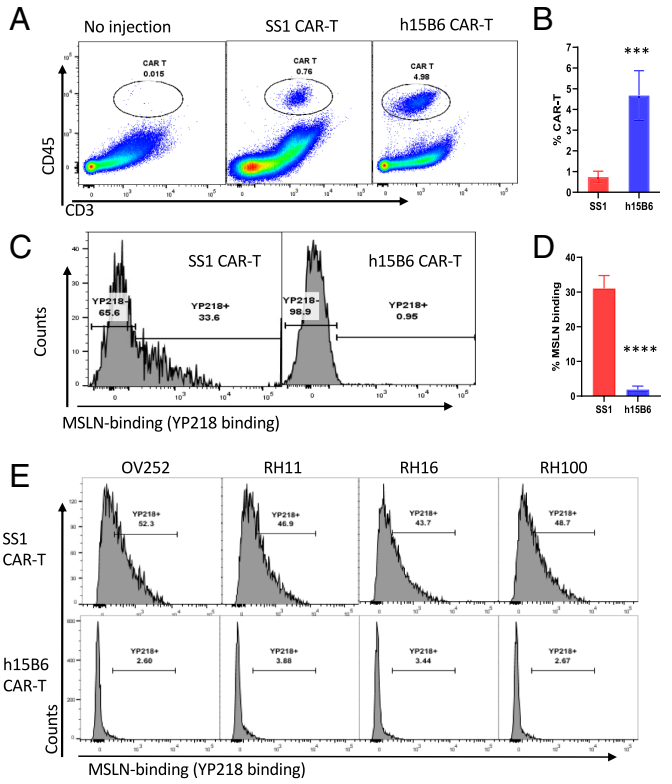

Fig. 4. Binding of shed MSLN to CAR-T cells: h15B6 CAR-T cells in mouse ascites do not contain shed-MSLN and do not bind to shed MSLN in ascites of patients. (*A* and *B*) Mice with OVCAR 8 I.P. tumors were treated 21 d after tumor implantation with either h15B6 or SS1 CAR-T. Seven days later, the cells in ascites were stained for anti-CD3 and anti-CD45. For flow analysis, live cells were first gated with DAPI; then, CD3 and CD45 double-positives cells were identified and are circled. (*B*) Percentage of CD3 and CD45 double-positive cells (n = 6). (*C*) CD3 and CD45 double-positive cells from *A* were analyzed for binding to YP218-Alexa 647. (*D*) Summary of MSLN containing cells identified by Mab YP218 from 2 different experiments (n = 6). (*E*) Ascites or pleural fluid from ovarian patient (OV252) or mesothelioma patients (RH11, RH16, and RH100) were incubated with either 15B6 or SS1 CAR-T cells. The presence of shed MSLN on the CAR-T cells was detected by YP218-alexa 647. Refer *SI Appendix*, Fig. S5 for CAR-T positive cell identification. $^{**}P < 0.01$; $^{***}P < 0.001$.

more relevant to humans with cancer (22, 23), we investigated a PDX model in which the tumors are derived from a patient with pancreatic ductal adenocarcinoma. Frozen tumor samples expressing MSLN were obtained from the NCI repository and directly injected into NSG mice. Groups of 7 mice were treated with saline, SS1 CAR-T cells, or h15B6 CAR-T cells, when the tumors were 50 mm (3) or larger in size. This protocol required staggering CAR-T cell injections because the tumor pieces grow at slightly different rates (Fig. 5). Tumor size was measured frequently for 60 d (Fig. 5 *A* and *B*). In all cases, the h15B6 CAR-T-treated tumors completely regressed, whereas the SS1 CAR-T-treated tumors did not respond and grew at the same rate as tumors treated with saline only. Fig. 5*B* shows the response of each mouse in one experiment. This type of experiment was repeated 3 times with identical results. One of the repeats is shown in *SI Appendix*, Fig. S6. Fig. 5*C* shows sections of tumors at different magnifications stained with H&E that were obtained at the end of the experiment. A scar with no tumor cells is present in the h15B6 CAR-T-treated tumors, whereas the tumors treated with saline or SS1 CAR-T are very large and show central necrosis often found in large tumors.

Histologic Analysis of PDX Cancers. A more detailed histologic analysis of these tumors is shown in Fig. 6. Fig. 6*A* shows that 7 d after CAR-T administration, the saline- and SS1 CAR-T-treated

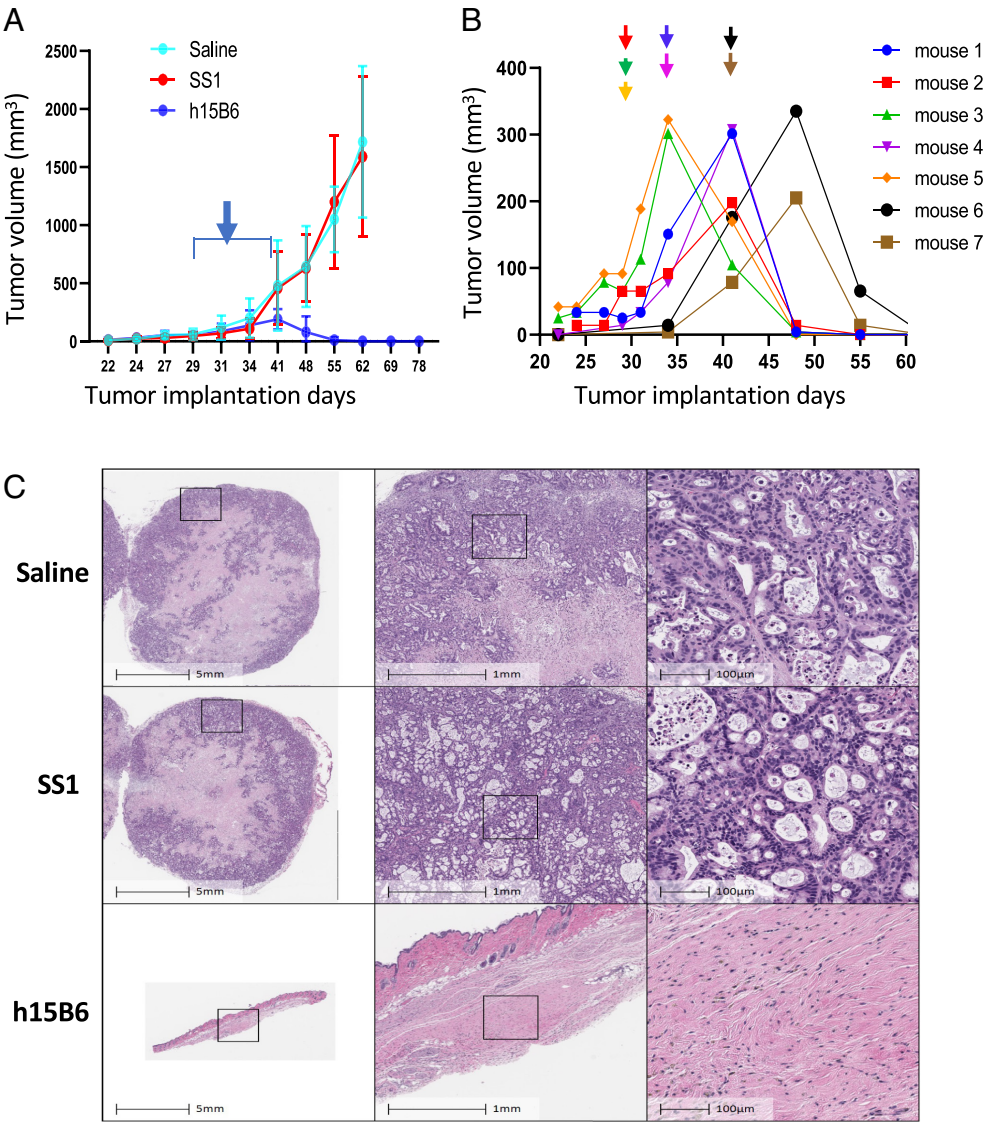

Fig. 5. Pancreatic Cancer PDX studies in mice. Human PDX pancreatic cancers were implanted subcutaneously, and the mice were treated with CAR-T cells when tumors reached 50 mm^3. (*A*) Average tumor volume: arrow indicates injection periods; 7 mice / group. (*B*) Individual mouse response to h15B6 CAR-T treatment. Arrows indicate the injection days for individual mice. (*C*) H.E. staining of xenografts of saline- and SS1 CAR-T-treated mice showing characteristic central necrosis at the end point. A collagenous scar is all that remains in the 15B6-treated mice.

tumors have nests of tumor cells in a dense stroma, whereas in the h15B6 CAR-T-treated tumors, the tumor cells are replaced with small inflammatory cells that are CD3-positive (Fig. 6*B*). Fig. 6*A* also shows that the large tumors in the saline and SS1 CAR-T groups stained very strongly for the tumor marker Cytokeratin 19, whereas very few Cytokeratin 19–positive cells were present on day 7 in the h15B6 CAR-T group. The SS1 CAR-T-treated tumors also stained strongly for MSLN but very weakly for human cells expressing CD3, CD4, or CD8 (Fig. 6*B*). The tumors from the h15B6 CAR-T mice had lost almost all MSLN expression and contained large numbers of CD3 cells which were a mixture of CD4 and CD8 cells.

h15B6 CAR-T Cells Replicate in Regressing Pancreatic Cancer. To determine whether the 15B6 CAR-T cells were replicating within the tumor, immunofluorescence with antibodies labeled with different fluorescent tags was employed. Fig. 7*A* (merged image) shows that CAR-T cells, identified with DAPI staining of the nucleus, are reactive for Ki67 that identifies replicating cells and for CD3 that reacts with the h15B6 CAR-T cells. Other panels show staining with DAPI or individual antibodies. This result clearly demonstrates that the 15B6 CAR-T cells are replicating inside the tumor. Fig. 7*B* shows that the SS1 CAR-T-treated tumors are mostly composed of replicating tumor cells that are DAPI and Ki67 positive, whereas very few tumor cells remain in the h15B6 CAR-T-treated group and are replaced by CD3-positive, Ki67-positive CAR-T cells.

Discussion

We have produced humanized CAR-T cells that target a membrane proximal epitope on MSLN. The h15B6 CAR-T have high anti-tumor activity in several tumor models and do not bind to shed MSLN allowing them to reach and kill MSLN-positive cells inside tumors. CAR-T cells targeting a distal epitope are bound to shed MSLN and do not accumulate in tumors (Fig. 1 *A* and *B*).

To enable the development of 15B6 CAR-T cells for clinical use, it was necessary to humanize the mouse Fv. We tried several approaches to achieve Fv humanization and found that using the closest human germline sequences as a guide was the most successful (Fig. 1*C* and *SI Appendix*, Fig. S1). The h15B6 CAR-T cells are indistinguishable in activity from CAR-T cells made with the mouse Fv in cell killing and in anti-tumor activity in mice (Fig. 2).

To determine whether the h15B6 CAR-T are active in a PDX tumor model in which the human tumors rather than cancer cell lines are implanted directly into mice, we implanted a PDX

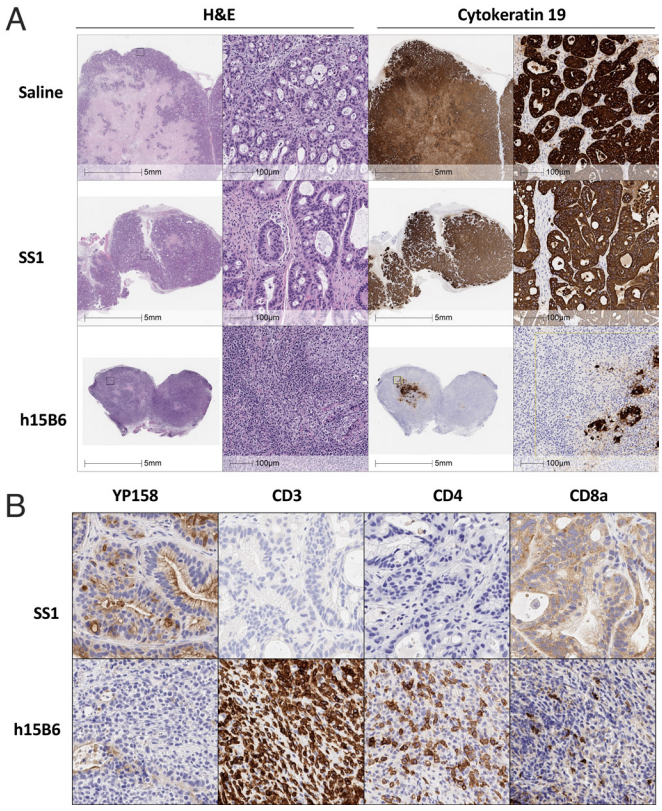

Fig. 6. Histological Analysis of PDX tumors. (*A*) H and E analysis on day 7 shows glandular structures that are Cytokeratin 19 positive in saline and SS1 CAR-T cells groups as well as dense matrix. h15B6 CAR-T-treated tumors show infiltration with inflammatory cells and very few remaining Cytokeratin-positive tumor cells. (*B*) Antibody staining of tumors shows that SS1 CAR-T tumors are MSLN positive (YP158) and CD3, CD4, and CD8 negative. H15B6 CAR-T-treated tumors are MSLN negative and very positive for CD3, CD4, and CD8.

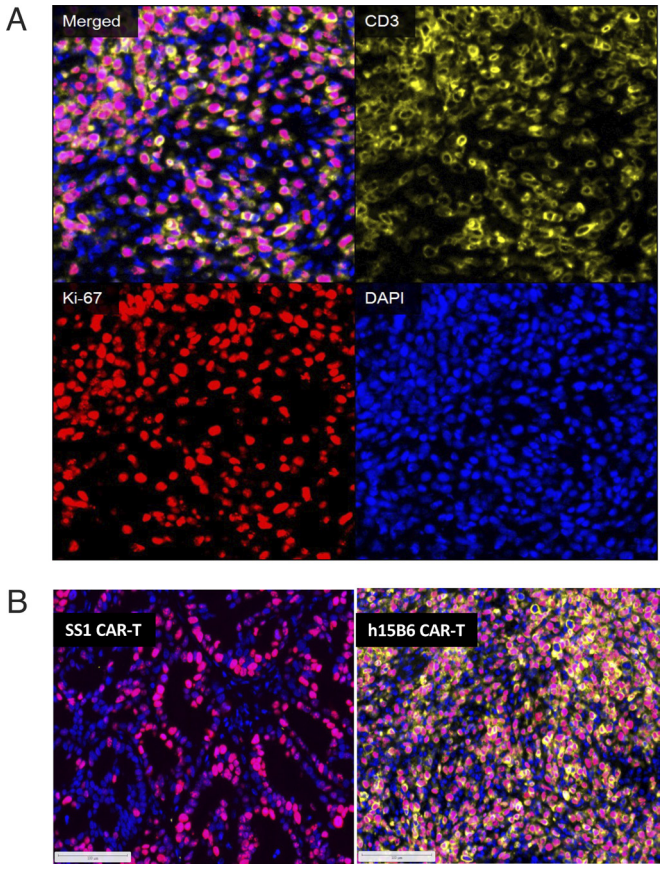

Fig. 7. Proliferation of h15B6 CAR-T cells in PDX pancreatic cancers on 7-d treatment time point. (*A*) Immunofluorescence study showing colocalization of Ki-67 (red) and CD3 (yellow) and DAPI (red) merged image (pink) in PDX cancers. (*B*) Fig. 6*B* shows that the SS1 CAR-T-treated tumors are mostly composed of replicating tumor cells that are DAPI and Ki67 positive. Very few tumor cells are present in the h15B6 CAR-T-treated group, and CD3-positive, Ki67-positive cells are present. Ki-67 positivity (pink) in neoplastic ductal epithelium in the SS1 CAR-T-treated mice and Ki-67 (pink) positivity in CAR-T cells (yellow) in the h15B6 CAR-T-treated mice.

pancreatic cancer in NSG mice (Figs. 5*C* and 6) and treated the mice when the tumors were 50 mm^3 or larger. We observed that h15B6 CAR-T cells produce complete and durable remissions in all (21/21) treated mice, whereas SS1 CAR-T cells have no anti-tumor activity. The data from 7 mice are shown in Fig. 5 and another 7 mice in *SI Appendix*, Fig. S4. When examined on day 60, the 15B6 CAR-T-treated mice contained a scar at the tumor site that consists mainly of fibroblasts with no evidence of any remaining cancer cells. This establishes the long-term effectiveness of this treatment.

Several proteins are made in large amounts by cancer cells and are shed into the blood; these include MUC16 (CA-125), CEA, and MSLN (24–27). All 3 are linked to the cell surface by phosphatidyl inositol. Antibodies against these proteins have been developed for therapeutic purposes, but their activity can be blocked by shed protein (25). To overcome this barrier, we identified the major forms of shed MSLN in blood, cell culture, and ascites and used this information to produce Mab 15B6 which reacts with Juxta-membrane residues of MSLN not present in shed MSLN (17). In addition, shed MSLN does not block the cell killing activity in vitro of CAR-T cells made with mab 15B6 (17).

Previous in vitro studies showed that binding to shed MSLN blocks the activity of SS1-CAR-T cells targeting an epitope in both shed and cell-bound MSLN. To determine whether we could directly demonstrate that poorly active CAR-T cells in mice are bound to shed MSLN, we analyzed CAR-T cells from ascites of mice with OVCAR-8 tumors by flow cytometry and found that very few h15B6 CAR-T cells contain shed MSLN, whereas many of the low-activity SS1-CAR-T have MSLN bound to them (Fig. 3). These mouse experiments confirm the prediction that shed MSLN, bound to SS1 CAR-T cells, prevents their cell killing action in mice (16). We assume that the same process will occur in humans because ascites fluid from patients with mesothelioma and ovarian cancer contains very high shed MSLN levels (in the μg/mL range) and shed MSLN can bind to SS1 but not 15B6 CAR-T cells (Fig. 7). Once inside the tumor, the h156B CAR-T cells multiply as shown in the pancreatic cancer PDX tumors and kill the target cells (Fig. 7). In contrast, the SS1 CAR-T cells do not accumulate in tumors, presumably because they do not receive a signal to expand which requires binding to cancer cells (Figs. 3 and 6). To determine experimentally whether the CAR-T cells retain proliferative capacity upon migration into the tumor, on day 7, we stained the sections from PDX tumors for CD3 to identify the CAR-T cells, for Ki-67 to identify dividing cells, and with DAPI to identify the nuclei. We found that most of the cells in the tumor are positive for all 3 markers, indicating that the CAR-T cells replicate inside the tumor.

A cartoon summarizing why h15B6 CAR-T cells have high anti-tumor activity and SS1-CAR-T have little or no anti-tumor activity in our mouse models is shown in Fig. 8. The *Upper* panel shows that shed MSLN in tumors is being released into capillaries. SS1-CAR-T cells in the capillaries encounter this MSLN as it leaves the tumor or as they enter the tumor. Although the shed

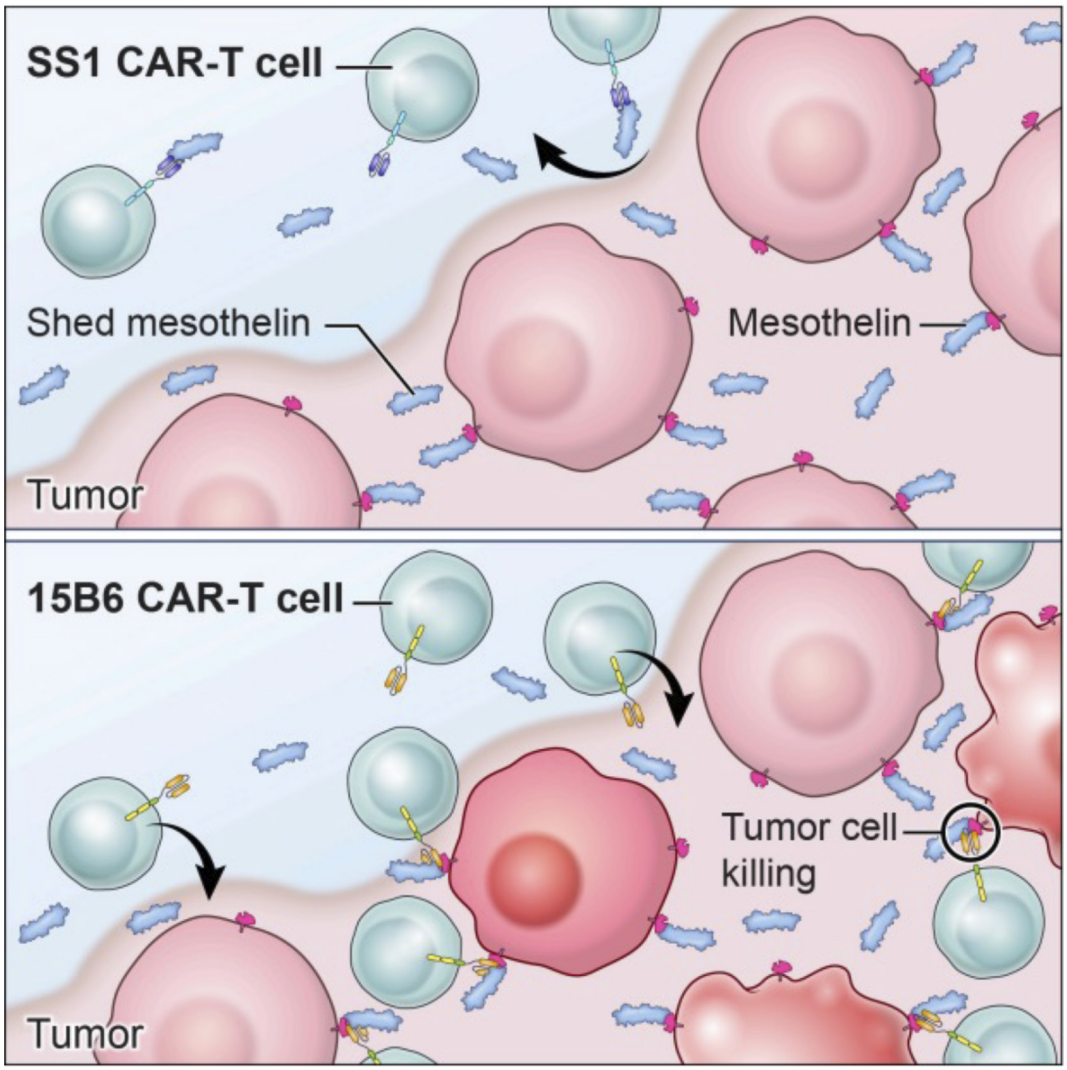

Fig. 8. Cartoon demonstrating why CAR-T cells targeting a distal MSLN epitope have very low anti-tumor activity and CAR-T targeting a non-shed epitope have high activity. MSLN (blue and red) on tumor cells is cut by proteases leaving a short stalk (red) attached to the cell and releasing the shed portion (blue) into the extra-cellular fluid of the tumor and then into the blood. CAR-T cells made with SS1 Fv recognize a distal epitope of MSLN present on shed MSLN, bind to shed MSLN as they enter the tumor or pass in capillaries through the tumor and do not accumulate in the tumor or reach tumor cells. CAR-T cells, made with 15B6 Fv, do not bind to shed MSLN. Therefore, after tumor entry, they can bind to and kill cancer cells. They are also activated and they expand as well.

MSLN levels in peripheral blood are low, the concentration in and emerging from the tumor must be much higher and is then diluted to the low levels found in peripheral blood. The *Lower* panel of Fig. 8 shows that h15B6 CAR-T cells do not bind to shed MSLN and are therefore able to enter the tumor and bind to and kill the tumor cells. This encounter also leads to CAR-T expansion within the tumor.

In summary, we have humanized the Fv of mab 15B6 so that CAR-T cells with the Fv can be used in patients. We then showed that the h15B6 CAR-T give complete remissions in a hard-to-treat pancreatic cancer PDX model, that the 15B6 CAR-T replicate within MSLN expressing cancers, and that in mice, there is shed MSLN bound to inactive SS1 CAR-T cells but not highly active 15B6 CAR-T cells. We believe that these data support the clinical development of h15B6 CAR-T for evaluation in patients.

Materials and Methods

Humanization of 15B6. Advice on humanization was provided by Roland Dunbrack, Fox Chase Cancer Center, and scientists at Absolute Antibody. The .pdb file for the model will be provided upon request.

Cell Culture. Early-passage mesothelioma cell lines were established from ascites or pleural fluid obtained from mesothelioma patients treated at the NCI (Bethesda, MD) on Institutional Review Board–approved Mesothelioma Natural History protocol (NCT01950572). The luciferase-expressing cell lines OVCAR-8-luc, KLM1-luc, A431-luc, RH29-luc, and KLM1 KO#2-luc were described before (17). All cells were cultured in RPMI-1640 medium. Culture media were supplemented with 10% FBS and 1% pen-strep. Cells were maintained at 5% Carbon Dioxide (CO_2) at 37 °C.

Generation and Expansion of CAR-T Cells. CAR-T cells were made as described before (17). Briefly, plasmids containing scFv in CAR-T vectors were packaged into lentivirus (Genetic Core NIH) and transducted into human PBMC stimulated with anti-CD3/CD28 Dynabeads (ThermoFisher). The transduced PBMCs were cultured with fresh medium containing 100U/ml IL-2 (Miltenyi Biotec) every other day. CAR-T cells were evaluated by double-positive staining of anti-CD3 and anti-EGFR by a flow cytometer. Cells were harvested around day 10 and frozen for later evaluation of toxicity study or animal injection. A total of 6 PBMCs were used throughout the study and all had similar cell killing activity.

Reagents Used by Flow Cytometry. FITC anti-human-CD3 (Cat:11-0036-42) and PE-anti-human-CD45 (Cat:12-0459-42) were purchased from ThermoFisher; PerCP anti-human CD45 Ab (Cat: 304026), APC anti-human CD3 Ab (Cat: 300312), and PE-anti-EGFR (Cat: FAB9577P) from R&D. YP218-Alexa647 were conjugated by using YP218 Ab with the protein labeling kit (ThermoFisher, Cat: A20186).

Luminescent-Based Cytolytic Assay. In vitro cell killing assay was described before (17). In short, different ratios of effector CAR-T cells were cocultured with luciferase expressing target cells in 96 well for 20 to 24 h. Cells were then lysed for 10 to 15 min in lysis buffer. The luciferase activity in the lysates was measured, and results were analyzed as percent killing: % killing = 100 − [relative light units (RLU) from wells with effector and target cells]/(Average RLU from wells with target cells) × 100.

NSG Mouse Tumor Treatment and Immunohistochemistry Analyses. Eight-to-ten-week-old immunologically deficient NOD.Cg-Prkdc^{scid} Il12rg^{tm1Wjl}/SzJ (hereafter NSG, Jackson Lab stock #005557) mice have been engrafted subcutaneously with a ~3 to 5-mm^3 fragment of PDX tumor tissue. When the tumor implants reached the size of 50 to 100 mm^3, animals have been randomized by tumor size into treatment groups and administered intravenously with a single dose of 200 μL saline or 1 × 10^7 SS1 or 15B6 CAR-T cells in 200 μL Roswell Park Memorial Institute Medium (RPMI) media. Upon the indicated time after treatment, tumors were excited and fixed in 10% NBF buffer for 48 h, dehydrated in 70% ethanol, and subsequently processed by either Histoserve, CAPR Histopathology group, or Molecular Histotechnology Laboratory (MHL) core facility in Frederick. Antibodies used for IHC: anti-human-CD3 is from BioRad (Cat #MCA1477, 1:100 dilution), anti-human-CD4 is from Abcam (Cat #ab133616, 1:250 dilution), anti-CD8a is from Thermo Fisher Scientific/eBioscience (Cat #14-0195-82, 1:50 dilution). For double immunofluorescent staining: anti-human CD3 antibody is from BioRad (Cat #MCA1477, 1:100 dilution), and anti-Ki67 antibody is from Cell Signaling Technologies, Inc. (Cat #9027, 1:250 dilution). Processed IHC and IF slides were scanned on bright-field or fluorescent Aperio Scanscope systems and representative images captured for all treatment groups. CD3-positive T cells were counted using HALO software by a pathologist in Frederick MHL core facility.

Mouse Blood and Spleen Cells Preparation for Flow Cytometer Studies. Mouse blood was collected from the facial vein directly in EDTA-coated tubes (Sarstedt, Catalog # 20.1278.100). Antibody cocktail with anti-human-CD3 or anti-human-CD45 was directly added to blood and incubated on ice for 30 min to 1 h. Samples were then washed with 0.3 mL Ammonium Chloride Potassium (ACK) lysis buffer (Thermo Fisher) and washed with 1.5 mL of fluorescence-activated cell sorting (FACS) buffer (PBS + 5% FBS). Spleen were collected from killed mice, they were then smashed into 45 μm filter, red blood cells were lysed using ACK lysis buffer, and ~ 500,000 cells were stained as human CD3 and human CD45. Live/dead cells were stained using 0.3 μg/mL DAPI. Samples were finally resuspended in 400 L of FACS buffer for processing in the flow cytometer.

Flow Cytometer Studies of Ascites. Ascites from control mice or tumor-bearing mice were killed by approved methods. Ascites was taken after injection of 5 mL phosphate-buffered saline (PBS) in peritoneal cavity. Cells were passed through a 40-μm filter to get rid of cell clusters. Red blood cells were lysed with ACK buffer if necessary. Cells then were stained with anti-CD3, anti-CD45, and YP218-Alexa 647 on ice and prepared for flow analysis. CAR-T cells were gated by double positive of human CD3 and human CD45. Ascites (RH11 and RH100) and pleural fluid (RH16) samples used in this study were obtained from patients with mesothelioma seen at the NIH, on an Institutional Review Board–approved protocol (ClinicalTrials.gov NCT01950572). Written informed consent was obtained before patients were enrolled on the study. The study was conducted in accordance with the principles of the International Conference on Harmonisation–Good Clinical Practice guidelines. Patient ascites (OV252, RH11, and RH100) or pleural fluid (RH16) were diluted 2 to 3 times with CAR-T cells and incubated on ice with anti-EGFR-PE and YP218-Alexa 647 for 1 h. CAR-T cells were gated with EGFR-PE. MSLN binding cells were gated as YP218-alexa647 positive cells. RH11 and RH16 were previously published (27).

Mass Photometry. Mass photometry was performed on the OneMP instrument (Refeyn, UK) according to the protocol published by the NIH National Heart, Lung, and Blood Institute Biophysics Core. In brief, protein stocks were diluted in PBS buffer and passed through a 0.22-μm filter. MSLN was mixed with either mouse 15B6 antibody (m15B6) or humanized 15B6 antibody (h15B6) at different concentrations (40 to 100 nM MSLN; 5 to 20 nM m15B6/h15B6) and incubated at room temperature for 5 min. The sample was loaded to the flow chambers, and over 500 particles were detected in 60 s for each acquisition. MP data points were converted to mass distribution using established calibration standards and processed using instrument software (DiscoverMP, Refeyn). Population fractions from three different concentrations were globally fitted to obtain binding kinetics with the lowest sum of squared error.

CAR-T Treatment of Tumors. Tumor implantation and CAR-T treatment were described as before (17). Briefly, 5 million tumor cells were implanted intraperitoneally (OVCAR-8) or subcutaneously (KLM1-luc) into 6 to 10-wk-old NSG mice. All tumor-bearing mice were injected with a single dose of 5 × 10^6 mock transfected T cells, SS1 CAR-T cells, or 15B6 CAR-T cells by the tail vein. Intraperitoneal OVCAR8 tumors were injected on days 21 to 22 and then imaged using Xenogen IVIS Lumina (PerkinElmer) every week. For the KLM1 subcutaneous model, tumor volume was measured by caliber every 3 d. All mice were housed and treated under the protocol approved by the Institutional Animal Care and Use Committee at the NIH.

Statistical Analysis. All data analysis was performed using GraphPad Prism 9.0. Unpaired Student's test was used to compare differences between groups. All the experiments were repeated at least two times.

Data, Materials, and Software Availability. All study data are included in the article and/or *SI Appendix*. The model is available in ModelArchive at https://www.modelarchive.org/doi/10.5452/ma-6i642 (28).

ACKNOWLEDGMENTS. We thank Emily Danoff, LMB, for assistance with experiments; Absolute Antibody and Ronald Dunbrack for suggestions on humanization; pathologist Baktiar Karim for analysis of staining of the tumor samples; and Donna Butcher for assistance with immunostaining. We thank the NCI Flow Cytometry Core Facility for the use of their facilities. We would like to thank the Biophysics Core Facility at the National Heart, Lung, and Blood Institute from the NIH for their support and assistance in mass photometry and Dr. Annunziata, NCI, for supplying samples. This research was supported by the Intramural Research Program of the NIH, National Cancer Institute, Center for Cancer Research. Molecular graphics images were produced using the UCSF Chimera package from the Resource for Biocomputing, Visualization, and Informatics at the University of California, San Francisco (supported by NIH P41 RR001081).

1. Y. Zou, W. Xu, J. Li, Chimeric antigen receptor-modified T cell therapy in chronic lymphocytic leukemia. *J. Hematol. Oncol.* **11**, 130 (2018).
2. R. Kai, M. D. Jain, E. L. Smith, Mechanisms of resistance and treatment of relapse after CAR-T-cell therapy for large B-cell lymphoma and multiple myeloma. *Transplant. Cell. Ther.* **29**, 418–428 (2023), 10.1016/j.jtct.2023.04.007.
3. S. S. Neelapu *et al.*, Axicabtagene ciloleucel CAR-T-cell therapy in refractory large B-cell lymphoma. *N. Engl. J. Med.* **377**, 2531–2544 (2017).
4. M. P. Jogalekar *et al.*, CAR-T-Cell-Based gene therapy for cancers: New perspectives, challenges, and clinical developments. *Front. Immunol.* **13**, 925985 (2022).
5. S. Ma *et al.*, Current progress in CAR-T cell therapy for solid tumors. *Int. J. Biol. Sci.* **15**, 2548–2560 (2019), 10.7150/ijbs.34213.
6. K. Chang, I. Pastan, M. C. Willingham, Isolation and characterization of a monoclonal antibody, K1, reactive with ovarian cancers and normal mesothelium. *Int. J. Cancer* **50**, 373–381 (1992).
7. R. Hassan *et al.*, Mesothelin immunotherapy for cancer: Ready for prime time? *J. Clin. Oncol.* **34**, 4171–4179 (2016).
8. A. Morello, M. Sadelain, P. S. Adusumilli, Mesothelin-targeted CARs: Driving T cells to solid tumors. *Cancer Discov.* **6**, 133–146 (2016).
9. A. Klampatsa, V. Dimou, S. M. Albelda, Mesothelin-targeted CAR-T cell therapy for solid tumors. *Expert Opin. Biol. Ther.* **21**, 473–486 (2021).
10. S. Tomar *et al.*, Development of highly effective anti-mesothelin hYP218 chimeric antigen receptor T cells with increased tumor infiltration and persistence for treating solid tumors. *Mol. Cancer Ther.* **21**, 1195–1206 (2022).
11. P. S. Adusumilli *et al.*, A phase I trial of regional mesothelin-targeted CAR T-cell Therapy in patients with malignant pleural disease, in combination with the anti-PD-1 agent pembrolizumab. *Cancer Discov.* **11**, 2748–2763 (2021).
12. Y. Zhang, L. Xiang, R. Hassan, I. Pastan, Immunotoxin and Taxol synergy results from a decrease in shed mesothelin levels in the extracellular space of tumors. *Proc. Natl. Acad. Sci. U.S.A.* **104**, 17099–17104 (2007).
13. Y. Zhang, O. Chertov, J. Zhang, R. Hassan, I. Pastan, Cytotoxic activity of immunotoxin SS1P is modulated by TACE-dependent mesothelin shedding. *Cancer Res.* **71**, 5915–5922 (2011).
14. X. Liu, A. Chan, C. H. Tai, T. Andresson, I. Pastan, Multiple proteases are involved in mesothelin shedding by cancer cells. *Commun. Biol.* **3**, 728 (2020).
15. D. Yeo, L. Castelletti, N. van Zandwijk, J. E. J. Rasko, Hitting the Bull's-eye: Mesothelin's role as a biomarker and therapeutic target for malignant pleural mesothelioma. *Cancers (Basel)* **13**, 3932 (2021).

16. Y. F. Zhang *et al.*, New high affinity monoclonal antibodies recognize non-overlapping epitopes on mesothelin for monitoring and treating mesothelioma. *Sci. Rep.* **5**, 9928 (2015).
17. X. Liu *et al.*, Highly active CAR T cells that bind to a juxta membrane region of mesothelin and are not blocked by shed mesothelin. *Proc. Natl. Acad. Sci. U.S.A.* **119**, e2202439119 (2022).
18. D. Wu, G. Piszczek, Rapid determination of antibody-antigen affinity by mass photometry. *J. Vis. Exp.* **8**, 10.3791/61784 (2021), 10.3791/61784.
19. L. R. Avula *et al.*, Mesothelin enhances tumor vascularity in newly forming pancreatic peritoneal metastases. *Mol. Cancer Res.* **18**, 229–239 (2020).
20. E. Hatterer *et al.*, Targeting a membrane-proximal epitope on mesothelin increases the tumoricidal activity of a bispecific antibody blocking CD47 on mesothelin-positive tumors. *MAbs.* **12**, 1739408 (2020).
21. J. Li *et al.*, Membrane-proximal epitope facilitates efficient T cell synapse formation by anti-FcRH5/CD3 and is a requirement for myeloma cell killing. *Cancer Cell* **31**, 383–395 (2017).
22. C. Chao *et al.*, PAtient-derived xenografts from colorectal carcinoma: A temporal and hierarchical study of murine stromal cell replacement. *Anticancer Res.* **37**, 3405–3412 (2017).
23. W. M. van Weerden, Patient-derived xenograft models in cancer research. *Cancers (Basel)* **13**, 815 (2021).
24. P. Conaghan *et al.*, Targeted killing of colorectal cancer cell lines by a humanised IgG1 monoclonal antibody that binds to membrane-bound carcinoembryonic antigen. *Br. J. Cancer* **98**, 1217–1225 (2008).
25. G. C. Ghedini *et al.*, Shed HER2 extracellular domain in HER2-mediated tumor growth and in trastuzumab susceptibility. *J. Cell Physiol.* **225**, 256–265 (2010), 10.1002/jcp.22257.
26. Y. Zhang, I. Pastan, High shed antigen levels within tumors: An additional barrier to immunoconjugate therapy. *Clin. Cancer Res.* **14**, 7981–7986 (2008), 10.1158/1078-0432.
27. J. Zhang *et al.*, Loss of mesothelin expression by mesothelioma cells grown in vitro determines sensitivity to anti-mesothelin immunotoxin SS1P. *Anticancer Res.* **32**, 5151–5158 (2012).
28. C.-H. Tai, I. Pastan, ma-6i642 humanized 15B6. ModelArchive. https://www.modelarchive.org/doi/10.5452/ma-6i642. Deposited 28 December 2023.